frontiers | Frontiers in Earth Science

TYPE Original Research
PUBLISHED 05 April 2023
DOI 10.3389/feart.2023.1171456

OPEN ACCESS

EDITED BY
Fan Yang,
Lanzhou University, China

REVIEWED BY
Xiaoqiang Zhu,
Anhui Normal University, China
Fei Xue,
Hohai University, China
Peng-Peng Yu,
Sun Yat-sen University, China

*CORRESPONDENCE
Leilei Dong,
leileidong@ustb.edu.cn

SPECIALTY SECTION
This article was submitted to Structural Geology and Tectonics, a section of the journal Frontiers in Earth Science

RECEIVED 22 February 2023
ACCEPTED 17 March 2023
PUBLISHED 05 April 2023

CITATION
Dong L, Bai X, Song M and Wang R (2023), Crustal thickness of the Jiaodong Peninsula in the Mesozoic: Implications for the destruction of the North China Craton.
Front. Earth Sci. 11:1171456.
doi: 10.3389/feart.2023.1171456

Crustal thickness of the Jiaodong Peninsula in the Mesozoic: Implications for the destruction of the North China Craton

Leilei Dong[1]*, Xin Bai[1], Mingchun Song[2] and Runsheng Wang[3]

[1]School of Civil and Resource Engineering, University of Science and Technology Beijing, Beijing, China, [2]College of Earth Sciences, Heibei GEO University, Shijiazhuang, Hebei, China, [3]Shandong Geophysical and Geochemical Exploration Institute, Jinan, China

The North China Craton underwent extensive and widespread crustal reworking (or decratonization) during the Mesozoic. However, how the decratonization operated is not well understood. Zircon compositions are widely used by the scientific community to reconstruct crustal thicknesses. In this study, we sampled 13 magmatic rocks in the Jiaodong Peninsula and used zircon Eu/Eu* to constrain the crustal thickness of the Jiaodong area and reveal decratonization processes in the Mesozoic time. The reconstructed crustal thickness using zircon Eu/Eu* is approximately 70 km in the Jurassic, and this value is 89 km at around 130 Ma, after which the crustal thickness drops to 30–40 km at ca. 110 Ma. These results are generally compatible with or slightly higher than the calculation results using a whole-rock La/Yb proxy for the Jurassic and ~130 Ma rocks. Crustal thickness estimated using a whole-rock La/Yb proxy for the ~110 Ma rocks is thicker than 70 km, which is not consistent with the geological facts and the result given by zircon proxy. The whole-rock proxy failed in estimating crustal thickness because of amphibole fractionation for the ~110 Ma rocks. The crustal thickening from Jurassic to ~130 Ma was probably related to the westward subduction of the Paleo-Pacific slab. The thinning of the crust from 130 to 110 Ma is not a rapid process but occurs more slowly than expected, which might be explained by the chemical erosion process rather than a mechanical delamination model. The chemical erosion was most likely induced by a rollback of the subducting slab and an upwelling of the asthenosphere.

KEYWORDS

North China Craton, zircon Eu/Eu*, crustal thickness, Jiaodong, Mesozoic

1 Introduction

Crustal thickness exerts critical controls on the magmatic differentiation (Lee and Anderson, 2015; Tang et al., 2018), paleo-climate (Ernst, 2010), and even the compositions of the continental crust (Lee and Anderson, 2015). A better understanding of the crustal thickness in geological history thus helps us develop a comprehensive knowledge of crustal evolution. The North China Craton (NCC) was a stable craton before the Late Paleozoic, but it underwent extensive thinning during the Mesozoic (Yang J.-H. et al., 2018; Wu et al., 2019; Zheng et al., 2021), producing a relatively thin lithosphere at its eastern part. Its refractory, cold, and thick lithosphere (>200 km) was removed and replaced by a juvenile, fertile, and thin (80–100 km) one (Menzies et al., 1993; Xu, 2001; Wu et al., 2019). This process is called decratonization or destruction of the craton (Yang J. et al., 2012; Zhu et al., 2017; Yang et al.,

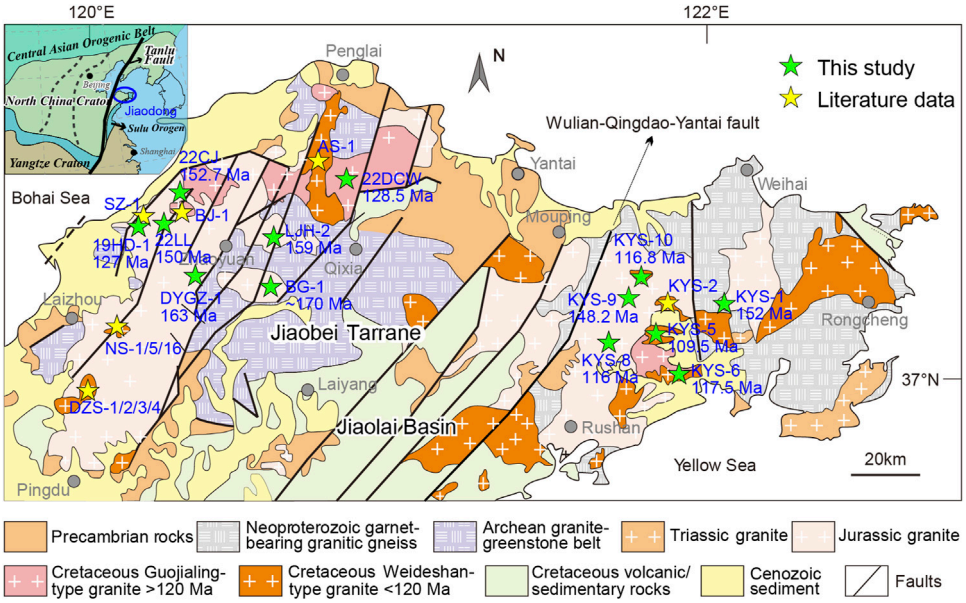

FIGURE 1
Geological map of the Jiaodong Peninsula showing major structures and lithological units (Song et al., 2015). The yellow stars represent the compiled published zircon data, while the green stars are data obtained in this study. Zircon ^{206}Pb-^{238}U ages are also shown after each sample. Inset showing the brief tectonic framework of the NCC.

2018b; Yang J.-H. et al., 2018; Ma et al., 2019). The decratonization was accompanied by strong crustal deformation (Zhu et al., 2009; Lin et al., 2013), widespread magmatism (Wu et al., 2005; Yang et al., 2018a), and gold mineralization (Deng et al., 2020). It has also been proposed that the lower crust of the NCC probably descended along with the lithosphere mantle into the asthenosphere, leading to the crustal thinning of eastern China (Gao et al., 2004; Hou et al., 2007; Ma et al., 2019). However, the thinning processes of the mantle + crust are not well understood because there are still debates on how the thinning operates. Two main models have been proposed: prolonged thermal processes (chemical erosion by the upwelling asthenosphere (Xu, 2001; Xu et al., 2009; Xue et al., 2019; Xue et al., 2021) and physical delamination caused by the orogenic collapse of the eclogitic crust and the lithosphere mantle (Gao et al., 2004). The former model implies a gradual process, while the latter favors rapid thinning. Crustal thinning and thickening processes are integral parts of the decratonization.

The Jiaodong Peninsula is located on the southeastern margin of the NCC. Many Mesozoic granitic intrusions are exposed at the surface, making it an ideal place for researching the topic of decratonization. The Jiaodong Peninsula records a holistic and complex magmatic process, which is reflected in the Mesozoic granitic rocks throughout the entire Jiaodong area. Whole-rock geochemical proxies were used to give constraints on the crustal thickness of the southeastern NCC (Zhang et al., 2008; Ma et al., 2013). Geochemical data suggested that eastern China, was a plateau during the Middle Jurassic to the Late Cretaceous period (Zhang et al., 2008). Recent studies argued that the Jurassic granitic rocks from the Jiaodong Peninsula and the northern margin of the NCC were generated by the melting of the thickened lower crust (Jiang et al., 2007; Ma et al., 2013; Li et al., 2019). A model that requires remelting of the descending eclogitic lower crust was invoked to explain the genesis of Early Cretaceous magmatic rocks (>120 Ma) (e.g., Hou et al., 2007). However, the crustal thickness of the eastern NCC during the Late Cretaceous period is not yet well constrained.

Zircon is widely used for dating, estimating magmatic oxidation states (Ballard et al., 2002; Loucks et al., 2020) and crystallization temperatures (Watson and Harrison, 2005), or indicating source rock types (Belousova et al., 2002; Yu et al., 2022; Mo et al., 2023). Zircon is ubiquitous in granitic rocks, and some researchers have used its trace element compositions to reconstruct crustal thickness (Tang et al., 2021). This method was also successfully applied to reveal the thickening history of the Central Andean Plateau (Sundell et al., 2022). The principle for using the zircon Eu/Eu* to infer the crustal thickness relies on the stability field of the plagioclase and garnet (Tang et al., 2021). Europium exists in the form of Eu^{2+} and Eu^{3+} in magmatic melt, while the proportion of each valence state depends on the relative oxidation state of the magma. The Eu^{2+} strongly partitions into plagioclase because Eu^{2+}, like the Sr^{2+}, has a similar ionic radius to Ca^{2+} (Shannon, 1976; Bédard, 2006). Therefore, melt generated in the plagioclase stable field or formed after plagioclase fractionation would be relatively depleted of Eu^{2+}, leading to a negative Eu anomaly and low Eu/Eu* in zircon (Tang et al., 2021). Such a process requires that this happens at geologically lower pressures (Moyen, 2009), corresponding to lower crustal levels (at a depth <45 km) (Qian and Hermann, 2013). In contrast, if the melt is formed in the garnet stable field (i.e., high pressure, commonly >15 kbar), garnet would sequester the Fe^{2+} from the melt and yield an oxidized environment (Tang et al., 2018; Tang et al., 2020), and this finally enriches the melt in Eu^{3+}. Zircon formed under such an oxidizing condition is capable of incorporating more Eu because Eu^{3+} is significantly more

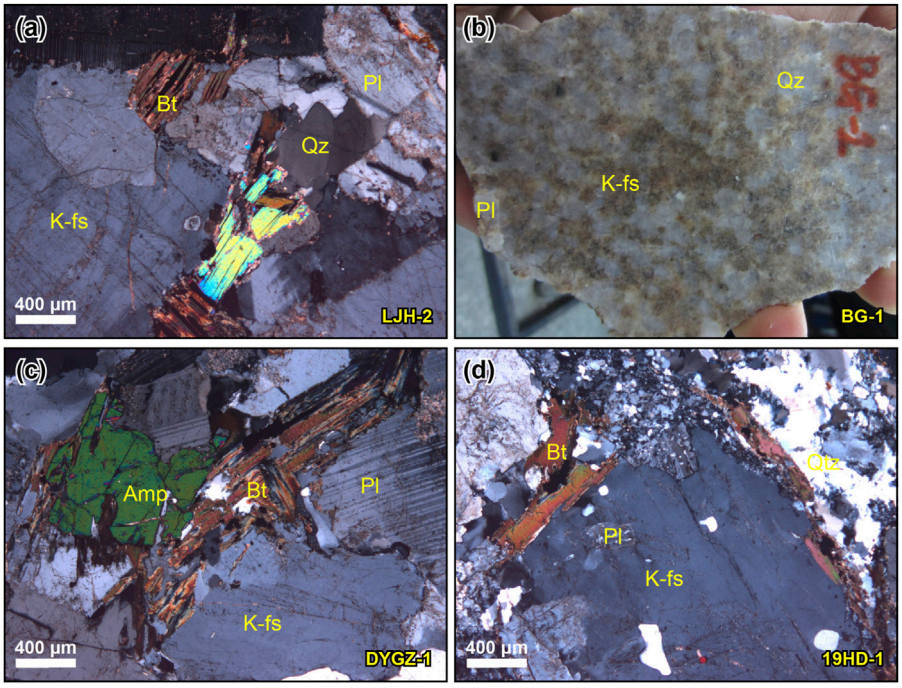

FIGURE 2
Microphotographs **(A, C, D)** and hand sample **(B)** of granitic rocks from the Jiaobei Terrane. **(A–C)** Samples from the Jurassic Luanjiahe, Biguo, and Linglong granites, respectively. **(D)** Early Cretaceous (>120 Ma) granite from the Hedong gold mine. K-fs, K-feldspar; Pl, plagioclase; Qz, quartz; Bt, biotite; Amp, amphibole; Tn, titanite.

compatible than Eu^{2+} in a zircon lattice (Trail et al., 2012). Consequently, zircon formed within the thick crust (at a depth >45 km) is characterized by high Eu/Eu*.

In this study, we report the compositions of zircon grains from the Mesozoic magmatic rocks to constrain the changing crustal thickness of the Jiaodong Peninsula. The geological significance of the calculated crustal thickness is discussed to develop a better understanding of the destruction of the NCC.

2 Geological setting

The NCC itself was composed of eastern and western blocks, which were sutured by the Trans-North China Orogen during a Paleoproterozoic orogenic event (Zhao et al., 2005). The basement of the two blocks consists of variably exposed Archean to Paleoproterozoic metamorphic rocks, including TTG gneiss, granite, charnockite, migmatite, amphibolite, greenschist, pelitic schist, Al-rich gneiss (khondalite), banded iron formation (BIF), calc-silicate rock, and marble (Jahn et al., 1987; Zhao et al., 2005; Wang et al., 2017). The Archean basement of the western block is exposed at the northern part of the block, while the southern part of the block is covered by the Mesozoic to Cenozoic strata, particularly in the Ordos Basin. The exposed basement of the western block consists of Late Archean low-grade granite-greenstone and high-grade TTG gneiss and granulite terrains, which underwent a greenschist-to-granulite facies metamorphism at ~2.5 Ga (Liu et al., 1993). The collision between the two blocks was recorded by the regional high-grade metamorphic rocks with metamorphic age of ~1.85 Ga in the Trans-North China Orogen (Zhao et al., 2008; Trap et al., 2012). The eastern block of the NCC has a similar lithology to the western part and consists of an Early Archean to Paleoproterozoic basement, covered by Mesoproterozoic to Cenozoic supracrustal rocks. The oldest Early Archean rock is represented by the ~3.8 Ga trondhjemitic gneisses in the Anshan area (Liu et al., 1992), while the Middle to Late Archean basement rocks are TTG gneisses with variable metamorphic grades (greenschist to granulite facies) (Li et al., 2005). The Paleoproterozoic metamorphic rocks in the eastern block occur along its eastern margin, consisting mainly of greenschist to lower amphibolite facies metasedimentary and metavolcanic rocks.

The Jiaodong Peninsula is located on the southeastern margin of the NCC (Figure 1). The Tan-Lu fault displaced the Jiaodong Peninsula from the Dabie Orogen to its current location in the Early Cretaceous (Zhu et al., 2009). The Jiaodong Peninsula is composed of the Jiaobei Terrane and the Sulu Orogen, which is separated by the Wulian-Qingdao-Yantai fault (Figure 1). The Jiaobei Terrane is an integral part of the NCC and is mainly composed of Precambrian metamorphic units. The Neoarchean and Paleoproterozoic metamorphic units are Neoarchean Qixia TTG gneiss and Jiaodong Group biotite granulite, plagioclase amphibolite, amphibolite, and magnetite quartzite. Proterozoic metamorphic rocks (the Jingshan, Zhifu, and Fenzishan Group) are marble, graphite-bearing granulite, and gneiss. The Late Jurassic biotite granite (Linglong granite), the Early Cretaceous Guojialing, and the Aishan granodiorite subsequently intruded into these metamorphic units in the Mesozoic (Figure 1). The Linglong granite is an NNW-elongated magmatic complex with different mineral textures at various parts of the intrusive body. The

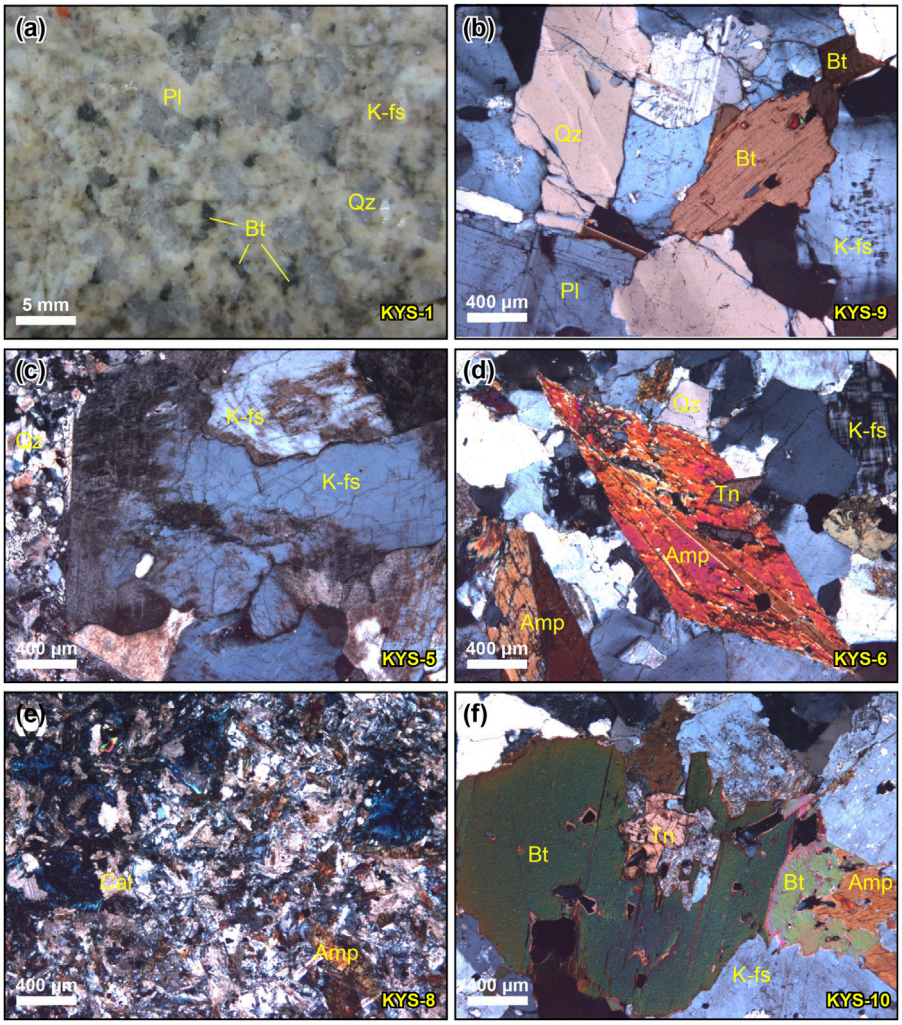

FIGURE 3
Hand sample **(A)** and microphotographs **(B–F)** of collected samples in the Kunyushan region. **(A–B)** KYS-1 and KYS-9 were collected from the Jurassic granite. **(C)** Porphyritic syenite. **(D)** Amphibole-bearing granite. **(E)** Basaltic andesite. **(F)** Amphibole-bearing granite. Cal, calcite. Other mineral abbreviations are the same as those in Figure 2.

published U-Pb ages of the Linglong granite range from ca. 170 to 140 Ma (Yang K. F. et al., 2012; Li et al., 2019; Dong et al., 2023a; Dong et al., 2023b). Several Early Cretaceous suites are, from west to east, Beijie, Shangzhuang, Congjia, and Guojialing granitoids, which are characterized by porphyritic texture with large K-feldspar phenocrysts. The U-Pb ages of these magmatic rocks are in the range of ca. 130–127 Ma (Li et al., 2019; Dong et al., 2023b). Another group of Early Cretaceous magmatic suites consists of Aishan, Nansu, and Dazeshan in the western part of the Jiaodong Peninsula, and the Weideshan, Yashan, and Longxudao plutons in the eastern Jiaodong, which are slightly younger than those of the former group (<120 Ma).

The Sulu Orogen, at the eastern side of the Wulian-Qingdao-Yantai fault, is a suture zone between the South China Block and the NCC. Within the suture zone, there are ultrahigh to high-pressure metamorphic rocks and Triassic K-rich shoshonitic rocks that represent a magmatic complex related to continental collision (Chen et al., 2003). This magmatic complex consists of pyroxene syenite, quartz syenite, and granite with zircon U-Pb ages of ca. 225–205 Ma (Chen et al., 2003). The Early Cretaceous volcanic and sedimentary rocks from the Jiaolai basin, with a maximum thickness of nearly 10 km, covered the southern part of the Jiaodong Peninsula. The lower part of the sequence is Laiyang Group clastic rocks, including sandstone, mudstone, and conglomerate. The Qingshan Group in the middle part of the sequence consists of dacite, andesite, and basalt. On the top of the sequence lies the Wangshi Group, which is composed of sandstone, mudstone, and conglomerate.

3 Samples and analytical methods

Thirteen samples were collected in this study (Figure 1). These samples include the Jurassic Linglong, Biguo, and Luanjiahe granites and the Guojialing, Congjia, and Shangzhuang granodiorites from the western part of the Jiaodong Peninsula, and the intrusive rocks in

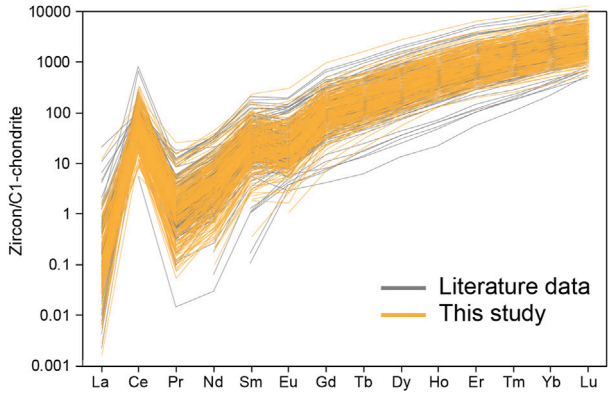

FIGURE 4
Zircon REE patterns normalized by C1-chondrite. For the three groups of zircons, the REE patterns are, in general, similar and are not further distinguished. The literature data source is Dong et al.; Dong et al., 2023b; Dong et al., 2023c.

the Kunyushan area of the Sulu Orogen. The mineral assemblages and textures of the magmatic rocks from the Jiaobei Terrane are well illustrated in previous studies (Dong et al., 2023b). Microphotographs and pictures of some representative samples are shown in Figure 2. Here we give a brief description of the samples from the Sulu Orogen (samples prefixed with KYS-).

Samples KYS-1 and KYS-9 were collected from the Jurassic granite, while the rest were sampled from the later intrusions (Figure 1). The Jurassic granite is light gray with equigranular texture (Figures 3A, B). Biotite, plagioclase, quartz, and K-feldspar are the major mineral phases. Sample KYS-5 is a porphyritic syenite dyke with K-feldspar phenocryst (Figure 3C). The KYS-6 is amphibole-bearing granite containing titanite as an accessory phase. The titanite crystals are enclosed by euhedral amphibole, indicating earlier crystallization (Figure 3D). The basaltic andesite (KYS-8) contains acicular amphibole and anhedral plagioclase (Figure 3E). Carbonate replacement of plagioclase is moderate in this sample. Sample KYS-10 is amphibole-bearing granite with minor accessory minerals like titanite (Figure 3F). The amphibole crystal is enclosed by K-feldspar and partially replaced by biotite.

Zircon grains from these magmatic rocks were separated using conventional heavy liquid and magnetic separation techniques. They were mounted in epoxy and surface polished. Transmitted, reflected light, and cathodoluminescence (CL) images were captured to acquire information about the inner structure, surface characteristics, and CL textures of the zircons, respectively. Laser ablation-inductively coupled plasma-mass spectrometry (LA-ICPMS) zircon U-Pb analyses were performed on an Agilent 7900 ICP-MS instrument equipped with a 193-nm laser ablation system at the Institute of Geology, Chinese Academy of Geological Sciences. Analytical locations were selected to avoid mineral inclusions and old inherited zircon cores. The laser was operated at an energy of 2 J/cm^2 and a repetition rate of 5 Hz, with a spot size of 30 μm. The ablated sample was transported into the ICP system *via* helium gas at a flow rate of 0.8 L/min. Immediately after the ablation, the He gas was mixed with Ar to improve transportation efficiency. Standard Zircon 91500 and GJ-1 samples were used for monitoring the precision and quality of the data.

4 Analytical results

Zircon U-Pb ages and trace element data are presented in the Supplementary Tables. Zircon U-Pb ages of samples from the same intrusion in the western part of the Jiaodong Peninsula give results that are identical to the published data. The oldest age obtained in this study is ~170 Ma (BG-1 from Biguo pluton). The rock with the youngest U-Pb age is quartz syenite from the Kunyushan region (KYS-5), which gives a weighted mean^{206}Pb-^{238}U age of 109.5 ± 0.7 Ma and a concordia age of 109.6 ± 0.7 Ma. The most mafic sample, KYS-8 (116.0 ± 0.7 Ma), is a diorite dyke intruding into the Jurassic Kunyushan composite complex with a weighted mean^{206}Pb-^{238}U age of 148.2 ± 1.1 Ma (KYS-9).

Rare earth elements (REEs) in zircon are characterized by enrichment in heavy REE relative to the light REE. Meanwhile, the Ce displays a positive anomaly in the C1-chondrite normalized patterns (Figure 4). However, the negative Eu anomaly is apparent in all the analyzed zircon grains. Hafnium contents are predominately within the range of 7,000–15,000 ppm for the Late Jurassic and Early Cretaceous zircon grains (Figure 5). We separated the zircon grains into three groups based on the zircon U-Pb ages of the related magmatic rocks: Late Jurassic zircon grains, Early Cretaceous zircon grains (>120 Ma), and Early Cretaceous zircon grains (<120 Ma). For the three groups of zircon grains, both the Eu/Eu* and Dy/Yb ratios display no obvious correlation with changing Hf contents (Figures 5A–F). Zircon Eu/Eu* values were calculated, where the Eu/Eu* represents the europium anomaly calculated as $Eu_N/(Sm_N \times Gd_N)^{0.5}$ and the subscript "N" denotes the chondrite normalized value from Sun and McDonough (1989). Zircon Eu/Eu* are mostly 0.2–0.8 for the Jurassic zircon grains (Figure 5A), whereas the Eu/Eu* are 0.6–1.0 for the Early Cretaceous (>120 Ma) zircon grains (Figure 5C). Zircon Eu/Eu* with ages younger than 120 Ma vary widely from 0.1 to 1.0 (Figure 5E). Zircon Dy/Yb ratios for the Late Jurassic and Early Cretaceous (<120 Ma) zircons are overall the same as the published data (Figures 5B, F), while the Dy/Yb values of Early Cretaceous (>120 Ma) zircon grains obtained in this study are generally lower than the published data (Figure 5D). Nonetheless, the zircon Dy/Yb ratios do not change much with increasing Hf concentrations in all three groups of zircon grains.

5 Discussion

5.1 Effect of fractionation on zircon Eu/Eu*

Although zircon is commonly an early crystallization phase in the melt, co-precipitation of certain accessory minerals, like titanite, competes for some elements and affects the zircon composition (e.g., Eu and Ta) (Chelle-Michou et al., 2014; Loader et al., 2017; Rezeau et al., 2019; Zou et al., 2019). Therefore, it is necessary to determine whether any of these minerals fractionated before or during zircon crystallization. Fractionation of plagioclase, titanite, and garnet probably affects the Eu content in the melt, resulting in changing

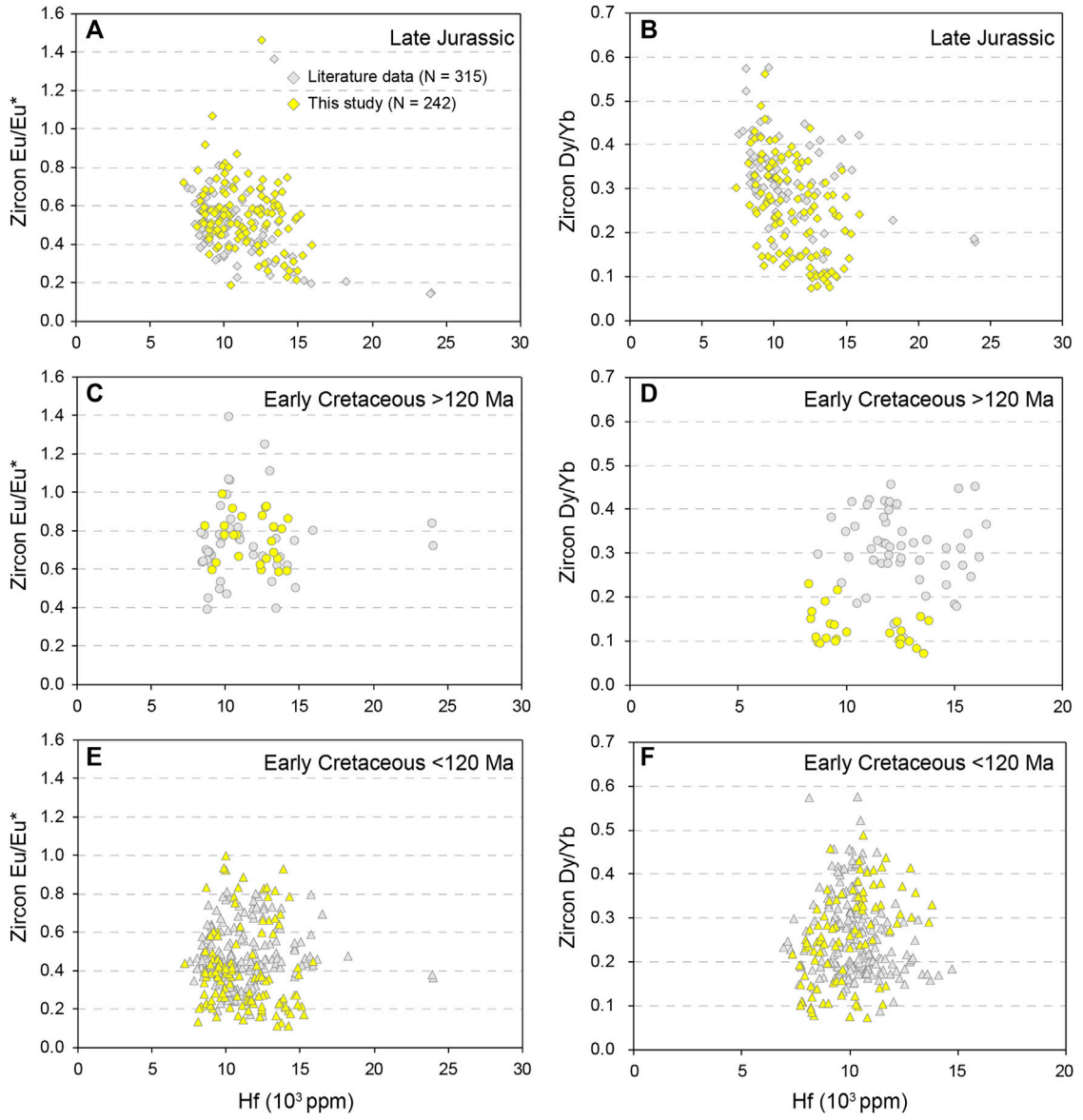

FIGURE 5
Zircon Eu/Eu* and Dy/Yb vs. Hf plots of Late Jurassic **(A, B)** and two groups of Early Cretaceous zircon grains **(C–F)** from all samples. The literature data source is the same as in Figure 4.

compositions of the subsequently crystallized zircon (Yu et al., 2019). Here, we use the zircon trace element concentrations to determine whether fractional crystallization of these minerals occurred during magmatic evolution. Eu/Eu* values in the Late Jurassic and Early Cretaceous zircons (both for the >120 Ma and <120 Ma) display insignificant increasing or decreasing trends with elevated Hf contents (Figures 5A, C, E), although there are large Eu/Eu* variations in these zircon grains. Compiled data also exhibit overlapping Eu/Eu* values and variational trends to our data (Dong et al., 2023a; Dong et al., 2023b). This would mean that there is no plagioclase fractionation after extraction of the melt and prior to the crystallization of zircon for all three groups of zircon grains. Garnet, which incorporates most of the heavy REE, can deplete the melt Yb content during fractionation (Green, 1994). The middle REEs (e.g., Dy) are more likely to partition into the amphibole (Davidson et al., 2007). Therefore, the zircon Dy/Yb effectively reveals the fractionation of these two minerals. The data from this study show that Dy/Yb ratios for the Late Jurassic zircons decrease with increasing Hf contents (Figure 5B). However, this trend is not apparent when considering all the zircon data from published literature (Dong et al., 2023a; Dong et al., 2023b). Dy/Yb ratios for the Early Cretaceous (>120 Ma) zircons remain constant with increasing Hf concentrations (Figure 5D). However, Dy/Yb ratios from this study are overall lower than the literature data. For another group of Early Cretaceous (<120 Ma) zircon grains, no correlation between the Dy/Yb and Hf is observed (Figure 5F). It is now concluded that

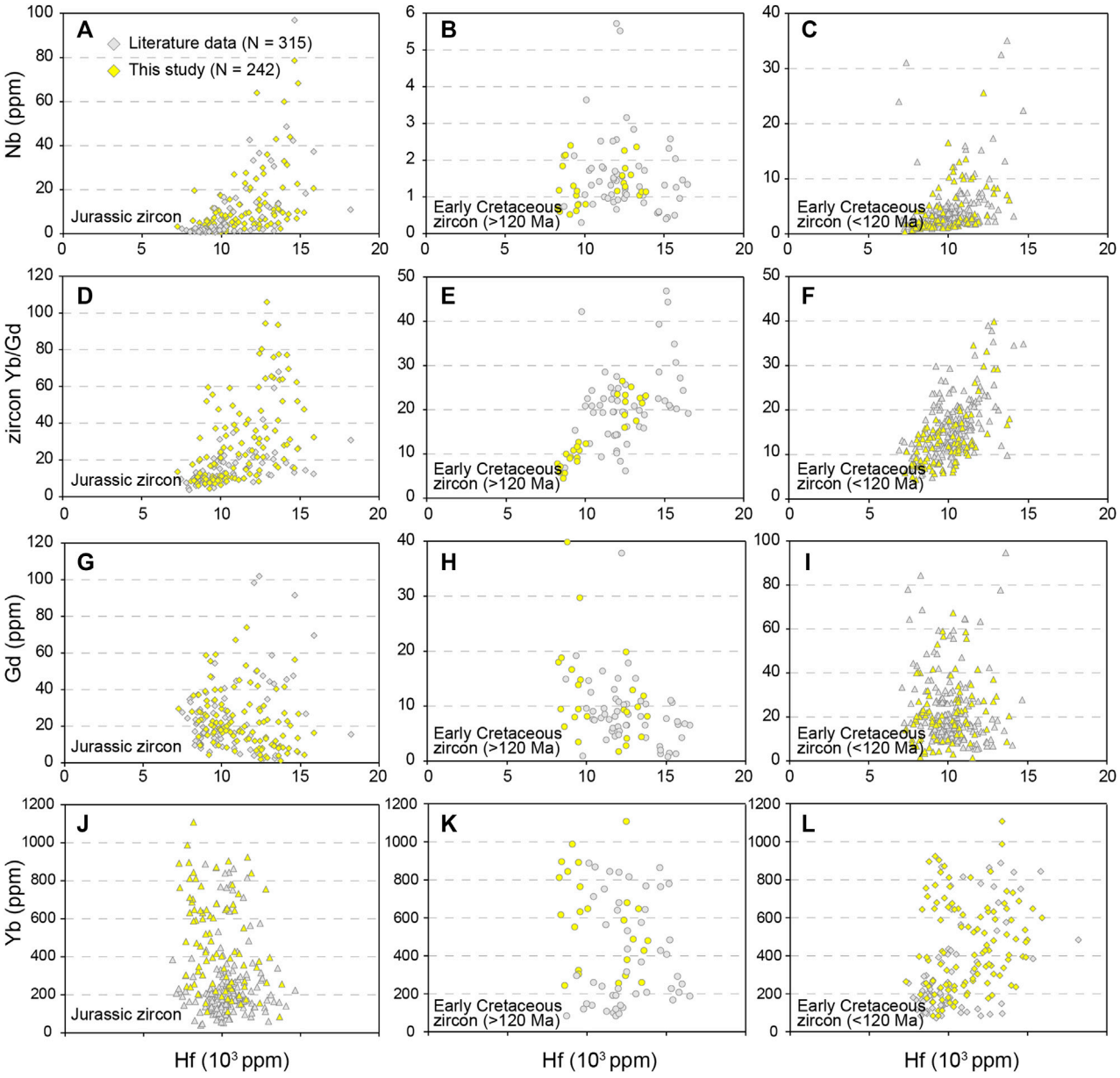

FIGURE 6
Nb **(A–C)**, Yb/Gd **(D–F)**, Gd **(G–I)**, and Yb contents **(J–L)** vs. Hf plots for the three groups of zircon grains from the studied samples. The literature data source is the same as in Figure 4.

fractionation of plagioclase, garnet, and amphibole is impracticable based on the aforementioned discussion.

Titanite, which commonly occurs as an accessory mineral in Early Cretaceous granitic rocks (Figure 3), could exert a pivotal influence on the middle REE over the heavy REE. Titanite fractionation leads to lower Ta and Nb concentrations and elevated Eu/Eu* in the residual melt, which would imprint these geochemical features on the subsequently crystallized zircon (Loader et al., 2017). Niobium concentrations in the Late Jurassic and Early Cretaceous (<120 Ma) zircons ascend from sub-ppm level to tens-of-ppm level with rising Hf contents (Figures 6A,C), while the Nb contents remain constant in the Early Cretaceous (>120 Ma) zircons (Figure 6B). This is the opposite of what would be expected when titanite fractionates from the melt. In the plots of zircon Yb/Gd vs. Hf (Figures 6D–F), Yb/Gd increases with rising Hf contents, which could be explained by increasing Yb or decreasing Gd in the melt or a combination of both. Notably, there are no such trends observed during magmatic evolution, as illustrated in Figure 6G–l. In addition, there is no amphibole or titanite fractionation, as indicated by the zircon Dy/Yb and Nb contents. In summary, it is inferred that no apparent crystal fractionation occurred when the three groups of zircon formed. The Eu/Eu* values recorded the original features of the melt when zircon formed.

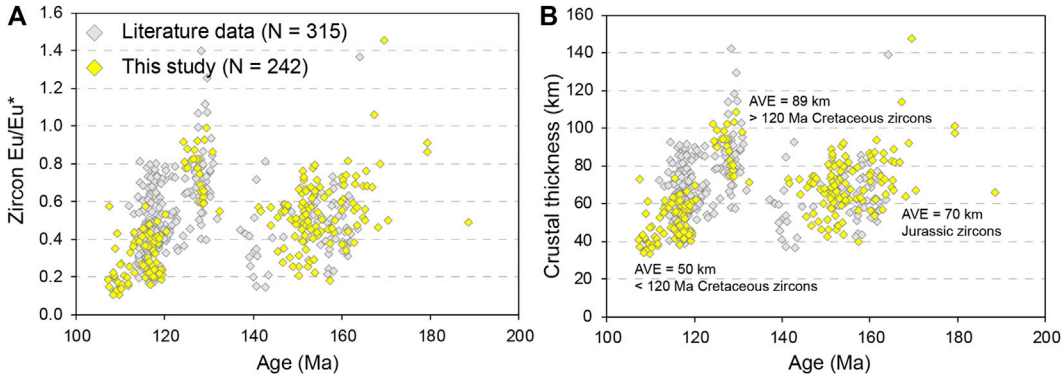

FIGURE 7
Plots of zircon Eu/Eu* **(A)** and reconstructed crustal thickness **(B)** vs. zircon ^{206}Pb-^{238}U ages from studied samples. The literature data source is the same as in Figure 4.

5.2 Changing crustal thickness of the Jiaodong Peninsula

Zircon Eu/Eu* values are plotted against the corresponding ^{206}Pb-^{238}U ages of each spot analysis (Figure 7A), and they show a weak correlation with the ages of the Jurassic zircon grains. However, an abrupt flare-up appears at ca. 130 Ma, after which zircon Eu/Eu* decreases at a high rate from 1.2 to 0.1. The changing pattern for the reconstructed crustal thickness mimics the zircon Eu/Eu* (Figure 7B). Average crustal thicknesses calculated using the zircon Eu/Eu* are 70 km in the Jurassic period, 89 km in the Early Cretaceous period (before 120 Ma), and 30–40 km at ca. 110 Ma. The crust was thick in the Jurassic, similar to the maximum crustal thickness in the current central Andes and Tibetan Plateau (Beck et al., 1996; Tang et al., 2021). This estimate is in accordance with the conclusion from geochemical data (high Sr/Y and La/Yb ratios for Jurassic Linglong granite), which indicates that a thick crust that stabilizes a large amount of garnet in the lower crust is required (Yang K. F. et al., 2012; Ma et al., 2013).

The reconstructed crustal thickness for the Jiaodong Peninsula at ca. 130 Ma is extremely high (~90 km), which is likely unrealistic because no modern example of such a thick crust has been reported. The possibility of this thick crust has not been evaluated. However, it is clear that the crustal thickness reaches its peak at ca. 130 Ma, according to this study. This estimated thickness agrees with the conclusion from geochemical modeling, which suggests that the magmatic suite formed at ca. 110 Ma was generated by the melting of the lower crust at moderate pressure (Dong et al., 2023c). Additionally, we also used the whole-rock La/Yb proxy (Profeta et al., 2015) to constrain crustal thickness for the three magmatic suites with published data (Yang K. F. et al., 2012; Ma et al., 2013; Li et al., 2019). The calculation results show that the average crustal thicknesses are 69 km (N=35), 85 km (N=28), and 78 km (N=24) for the Late Jurassic, Early Cretaceous (>120 Ma), and Early Cretaceous (<120 Ma) magmatic rocks, respectively. However, when using the method from Hu et al. (2017), average crustal thicknesses are 60 km, 80 km, and 72 km, respectively. The algorithm developed by Profeta et al. (2015) is based on whole-rock geochemical data from magmatic arcs, while the calculation method from Hu et al. (2017) is constructed using whole-rock geochemical data of collisional granites. The former gives higher values than the latter. The results for the former two magmatic suites are generally consistent with the results constrained with zircon Eu/Eu* proxy. However, the crustal thickness is too high for the <120 Ma magmatic rocks when using the whole-rock proxies. We would argue that the high crustal thickness given by whole-rock data probably results from the amphibole fractionation in the <120 Ma magmatic suites (Li et al., 2019). Because the amphibole fractionation could lower the Yb contents in the residue melt and further elevate the La/Yb ratio of the whole rock.

5.3 Decratonization of the NCC

Decratonization of the NCC is complex as there are many facts and conjectures on how this process operates (Wu et al., 2019). One school of thought argues that the decratonization happened rapidly through mechanical delamination of the old and refractory lithospheric mantle and the eclogitic lower crust (Gao et al., 2004; Ma et al., 2014; Yang J.-H. et al., 2018). Other researchers have proposed that the lithosphere mantle was chemically eroded by the convective asthenosphere mantle, which was a relatively gradual and slow process (Xu et al., 2009; Geng et al., 2019; Xue et al., 2021). Our results in this study demonstrate that the crust was thick before ca. 130 Ma, while the thickness reduced to about 30–40 km at ca. 110 Ma (Figure 7B). The crustal thickness at ca. 110 Ma was identical to the current thickness of the eastern NCC, as indicated by geophysical data (Zhang et al., 2014; Ma et al., 2019). This accordance further confirms that the zircon Eu/Eu* is robust in reconstructing crustal thickness. Therefore, it is concluded that the crustal thickness of southeastern NCC decreased from >70 km to 30–40 km over 20 million years, which is not a sudden transition. The crustal thickness probably decreased at a rate of 2.0–4.5 km/My.

The crustal thickness-zircon age correlation (Figure 7B) implies that, during 130–110 Ma, crustal thickness became thinner with decreasing age, which cannot be explained by the

mechanical delamination model. The descending lithosphere mantle and crust would have produced melt with "thicker crust" geochemical features as the source region for the magmatic rocks became deeper. In sum, we suggest that the decratonization was a slow process, and chemical erosion is the most plausible mechanism.

6 Conclusion

Based on the reconstruction of crustal thickness with zircon Eu/Eu* from the granitic rocks in the Jiaodong Peninsula, the following conclusions are derived.

(1) Crystal fractionation of minerals like titanite, plagioclase, and garnet is not significant and exerts no effect on the compositions of zircons.
(2) The crust of the Jiaodong Peninsula was thick (~70 km) during the Late Jurassic period (170–150 Ma) and reached its peak in the Early Cretaceous period (~130 Ma), while the crustal thickness decreased to approximately 30–40 km at ~110 Ma. These results are in agreement with the calculation using whole-rock La/Yb proxy.
(3) Decratonization of the NCC was not a sudden process but proceeded gradually, which should be reconciled by chemical erosion.
(4) It is suggested that whole-rock proxies for calculating crustal thickness are not applicable when there is obvious crystal fractionation (e.g., amphibole).

Data availability statement

The original contributions presented in the study are included in the article/Supplementary Material. further inquiries can be directed to the corresponding author.

Author contributions

LD and MS designed the project. LD and RW collected the samples and performed part of the experiment. XB performed some zircon dating work and data processing. XB and LD drafted the manuscript.

Funding

This study was financially supported by the National Natural Science Foundation of China-Shandong Joint Fund Program (U2006201) and Fundamental Research Funds for the Central Universities (FRF-TP-20-042A1).

Acknowledgments

The authors would like to express their sincere thanks to Li Huawei for helping with the LA-ICPMS zircon U-Pb analyses.

Conflict of interest

The authors declare that the research was conducted in the absence of any commercial or financial relationships that could be construed as a potential conflict of interest.

Publisher's note

Supplementary material

The Supplementary Material for this article can be found online at: https://www.frontiersin.org/articles/10.3389/feart.2023.1171456/full#supplementary-material

References

Ballard, J. R., Palin, M. J., and Campbell, I. H. (2002). Relative oxidation states of magmas inferred from Ce (IV)/Ce (III) in zircon: Application to porphyry copper deposits of northern Chile. *Contributions Mineralogy Petrology* 144, 347–364. doi:10.1007/s00410-002-0402-5

Beck, S. L., Zandt, G., Myers, S. C., Wallace, T. C., Silver, P. G., and Drake, L. (1996). Crustal-thickness variations in the central Andes. *Geology* 24, 407–410. doi:10.1130/0091-7613(1996)024<0407:ctvitc>2.3.co;2

Bédard, J. H. (2006). Trace element partitioning in plagioclase feldspar. *Geochimica Cosmochimica Acta* 70, 3717–3742. doi:10.1016/j.gca.2006.05.003

Belousova, E., Griffin, W., O'Reilly, S. Y., and Fisher, N. (2002). Igneous zircon: Trace element composition as an indicator of source rock type. *Contributions Mineralogy Petrology* 143, 602–622. doi:10.1007/s00410-002-0364-7

Chelle-Michou, C., Chiaradia, M., Ovtcharova, M., Ulianov, A., and Wotzlaw, J.-F. (2014). Zircon petrochronology reveals the temporal link between porphyry systems and the magmatic evolution of their hidden plutonic roots (the Eocene Coroccohuayco deposit, Peru). *Lithos* 198-199, 129–140. doi:10.1016/j.lithos.2014.03.017

Chen, J. F., Xie, Z., Zhang, X. D., Zhou, T. X., Park, Y. S., Ahn, K. S., et al. (2003). U-Pb zircon ages for a collision-related K-rich complex at Shidao in the Sulu ultrahigh pressure terrane, China. *Geochem. J.* 37, 35–46. doi:10.2343/geochemj.37.35

Davidson, J., Turner, S., Handley, H., Macpherson, C., and Dosseto, A. (2007). Amphibole "sponge" in arc crust? *Geology* 35, 787–790. doi:10.1130/g23637a.1

Deng, J., Yang, L., Groves, D., Zhang, L., Qiu, K.-F., and Wang, Q.-F. (2020). An integrated mineral system model for the gold deposits of the giant Jiaodong province, eastern China. *Earth-Science Rev.* 208, 103274. doi:10.1016/j.earscirev.2020.103274

Dong, L., Yang, Z., Bai, X., and Deng, C. (2023a). Generation of the early cretaceous granitoid in the dazeshan region, Jiaodong Peninsula: Implications for the crustal reworking in the North China craton. *Front. Earth Sci.* 10, 2444. doi:10.3389/feart.2022.1083608

Dong, L., Yang, Z., Liu, Y., and Song, M. (2023b). Possible source of Au in the Jiaodong area from lower crustal sulfide cumulates: Evidence from oxygen states and chalcophile elements contents of Mesozoic magmatic suites. *Ore Geol. Rev.* 153, 105268. doi:10.1016/j.oregeorev.2022.105268

Dong, L., Yang, Z., Song, M., and Bai, X. (2023c). Petrogenesis of mesozoic magmatic suites in the Jiaodong Peninsula: Implications for crust-mantle interactions and decratonization. *Lithosphere* 2023, 6226908. doi:10.2113/2023/6226908

Ernst, W. G. (2010). Young convergent-margin orogens, climate, and crustal thickness—a late cretaceous–paleogene nevadaplano in the American southwest? *Lithosphere* 2, 67–75. doi:10.1130/l84.1

Gao, S., Rudnick, R. L., Yuan, H.-L., Liu, X.-M., Liu, Y.-S., Xu, W.-L., et al. (2004). Recycling lower continental crust in the North China craton. *Nature* 432, 892–897. doi:10.1038/nature03162

Geng, X., Foley, S. F., Liu, Y., Wang, Z., Hu, Z., and Zhou, L. (2019). Thermal-chemical conditions of the North China Mesozoic lithospheric mantle and implication for the lithospheric thinning of cratons. *Earth Planet. Sci. Lett.* 516, 1–11. doi:10.1016/j.epsl.2019.03.012

Green, T. H. (1994). Experimental studies of trace-element partitioning applicable to igneous petrogenesis—sedona 16 years later. *Chem. Geol.* 117, 1–36. doi:10.1016/0009-2541(94)90119-8

Hou, M. L., Jiang, Y. H., Jiang, S. Y., Ling, H. F., and Zhao, K. D. (2007). Contrasting origins of late mesozoic adakitic granitoids from the northwestern Jiaodong Peninsula, east China: Implications for crustal thickening to delamination. *Geol. Mag.* 144, 619–631. doi:10.1017/s0016756807003494

Hu, F., Ducea, M. N., Liu, S., and Chapman, J. B. (2017). Quantifying crustal thickness in continental collisional belts: Global perspective and a geologic application. *Sci. Rep.* 7, 7058. doi:10.1038/s41598-017-07849-7

Jahn, B., Auvray, B., Cornichet, J., Bai, Y., Shen, Q., and Liu, D. (1987). 3.5 Ga old amphibolites from eastern hebei province, China: Field occurrence, petrography, Sm-Nd isochron age and REE geochemistry. *Precambrian Res.* 34, 311–346. doi:10.1016/0301-9268(87)90006-4

Jiang, N., Liu, Y., Zhou, W., Yang, J., and Zhang, S. (2007). Derivation of Mesozoic adakitic magmas from ancient lower crust in the North China craton. *Geochimica Cosmochimica Acta* 71, 2591–2608. doi:10.1016/j.gca.2007.02.018

Lee, C.-T. A., and Anderson, D. L. (2015). Continental crust formation at arcs, the arclogite "delamination" cycle, and one origin for fertile melting anomalies in the mantle. *Sci. Bull.* 60, 1141–1156. doi:10.1007/s11434-015-0828-6

Li, S., Zhao, G., Sun, M., Han, Z., Luo, Y., Hao, D., et al. (2005). Deformation history of the paleoproterozoic liaohe assemblage in the eastern block of the North China craton. *J. Asian Earth Sci.* 24, 659–674. doi:10.1016/j.jseaes.2003.11.008

Li, X.-H., Fan, H.-R., Hu, F.-F., Hollings, P., Yang, K.-F., and Liu, X. (2019). Linking lithospheric thinning and magmatic evolution of late Jurassic to early cretaceous granitoids in the Jiaobei Terrane, southeastern North China Craton. *Lithos* 324-325, 280–296. doi:10.1016/j.lithos.2018.11.022

Lin, W., Charles, N., Chen, Y., Chen, K., Faure, M., Wu, L., et al. (2013). Late mesozoic compressional to extensional tectonics in the yiwulüshan massif, NE China and their bearing on the yinshan–yanshan orogenic belt: Part II: Anisotropy of magnetic susceptibility and gravity modeling. *Gondwana Res.* 23, 78–94. doi:10.1016/j.gr.2012.02.012

Liu, D. Y., Nutman, A. P., Compston, W., Wu, J. S., and Shen, Q. H. (1992). Remnants of ≥3800 Ma crust in the Chinese part of the Sino-Korean craton. *Geology* 20, 339–342. doi:10.1130/0091-7613(1992)020<0339:romcit>2.3.co;2

Loader, M. A., Wilkinson, J. J., and Armstrong, R. N. (2017). The effect of titanite crystallisation on Eu and Ce anomalies in zircon and its implications for the assessment of porphyry Cu deposit fertility. *Earth Planet. Sci. Lett.* 472, 107–119. doi:10.1016/j.epsl.2017.05.010

Loucks, R. R., Fiorentini, M. L., and Henríquez, G. J. (2020). New magmatic oxybarometer using trace elements in zircon. *J. Petrology* 61. egaa034. doi:10.1093/petrology/egaa034

Ma, L., Jiang, S. Y., Dai, B. Z., Jiang, Y. H., Hou, M. L., Pu, W., et al. (2013). Multiple sources for the origin of Late Jurassic Linglong adakitic granite in the Shandong Peninsula, eastern China: Zircon U–Pb geochronological, geochemical and Sr–Nd–Hf isotopic evidence. *Lithos* 162-163, 251–263. doi:10.1016/j.lithos.2013.01.009

Ma, L., Jiang, S. Y., Hofmann, A. W., Dai, B. Z., Hou, M. L., Zhao, K. D., et al. (2014). Lithospheric and asthenospheric sources of lamprophyres in the Jiaodong Peninsula: A consequence of rapid lithospheric thinning beneath the North China craton? *Geochimica Cosmochimica Acta* 124, 250–271. doi:10.1016/j.gca.2013.09.035

Ma, Q., Xu, Y.-G., Deng, Y., Zheng, J.-P., Sun, M., Griffin, W. L., et al. (2019). Similar crust beneath disrupted and intact cratons: Arguments against lower-crust delamination as a decratonization trigger. *Tectonophysics* 750, 1–8. doi:10.1016/j.tecto.2018.11.007

Menzies, M. A., Fan, W., and Zhang, M. (1993). Palaeozoic and Cenozoic lithoprobes and the loss of >120 km of Archaean lithosphere, Sino-Korean craton, China. *Geol. Soc. Lond. Spec. Publ.* 76, 71–81.

Mo, J., Xia, X.-P., Li, P.-F., Spencer, C. J., Lai, C.-K., Xu, J., et al. (2023). Water-in-zircon: A discriminant between S- and I-type granitoid. *Contributions Mineralogy Petrology* 178, 5. doi:10.1007/s00410-022-01986-7

Moyen, J.-F. (2009). High Sr/Y and La/Yb ratios: The meaning of the "adakitic signature". *Lithos* 112, 556–574. doi:10.1016/j.lithos.2009.04.001

Profeta, L., Ducea, M. N., Chapman, J. B., Paterson, S. R., Gonzales, S. M. H., Kirsch, M., et al. (2015). Quantifying crustal thickness over time in magmatic arcs. *Sci. Rep.* 5, 17786. doi:10.1038/srep17786

Qian, Q., and Hermann, J. (2013). Partial melting of lower crust at 10–15 kbar: Constraints on adakite and TTG formation. *Contributions Mineralogy Petrology* 165, 1195–1224. doi:10.1007/s00410-013-0854-9

Rezeau, H., Moritz, R., Wotzlaw, J.-F., Hovakimyan, S., and Tayan, R. (2019). Zircon petrochronology of the meghri-ordubad pluton, lesser caucasus: Fingerprinting igneous processes and implications for the exploration of porphyry Cu-Mo deposits. *Econ. Geol.* 114, 1365–1388. doi:10.5382/econgeo.4671

Shannon, R. D. (1976). Revised effective ionic radii and systematic studies of interatomic distances in halides and chalcogenides. *Acta Crystallogr. Sect. A Cryst. Phys. Diffr. Theor. general Crystallogr.* 32, 751–767. doi:10.1107/s0567739476001551

Song, M.-c., Li, S.-z., Santosh, M., Zhao, S., Yu, S., Yi, P.-h, et al. (2015). Types, characteristics and metallogenesis of gold deposits in the Jiaodong Peninsula, Eastern North China Craton. *Ore Geology Reviews* 65 (3), 612–625.

Sun, S. s., and McDonough, W. F. (1989). Chemical and isotopic systematics of oceanic basalts: Implications for mantle composition and processes. *Geol. Soc. Lond. Spec. Publ.* 42, 313–345. doi:10.1144/gsl.sp.1989.042.01.19

Sundell, K. E., George, S. W., Carrapa, B., Gehrels, G. E., Ducea, M. N., Saylor, J. E., et al. (2022). Crustal thickening of the northern Central Andean Plateau inferred from trace elements in zircon. *Geophys. Res. Lett.* 49, e2021GL096443. doi:10.1029/2021gl096443

Tang, M., Erdman, M., Eldridge, G., and Lee, C.-T. A. (2018). The redox "filter" beneath magmatic orogens and the formation of continental crust. *Sci. Adv.* 4, eaar4444. doi:10.1126/sciadv.aar4444

Tang, M., Ji, W.-Q., Chu, X., Wu, A., and Chen, C. (2021). Reconstructing crustal thickness evolution from europium anomalies in detrital zircons. *Geology* 49, 76–80. doi:10.1130/g47745.1

Tang, M., Lee, C.-T., Ji, W.-Q., Wang, R., and Costin, G. (2020). Crustal thickening and endogenic oxidation of magmatic sulfur. *Sci. Adv.* 6, eaba6342. doi:10.1126/sciadv.aba6342

Trail, D., Bruce Watson, E., and Tailby, N. D. (2012). Ce and Eu anomalies in zircon as proxies for the oxidation state of magmas. *Geochimica Cosmochimica Acta* 97, 70–87. doi:10.1016/j.gca.2012.08.032

Trap, P., Faure, M., Lin, W., Le Breton, N., and Monié, P. (2012). Paleoproterozoic tectonic evolution of the Trans-North China Orogen: Toward a comprehensive model. *Precambrian Res.* 222-223, 191–211. doi:10.1016/j.precamres.2011.09.008

Wang, C., Peng, Z., Tong, X., Huang, H., Zheng, M., Zhang, L., et al. (2017). Late Neoarchean supracrustal rocks from the Anshan-Benxi terrane, North China Craton: New geodynamic implications from the geochemical record. *Am. J. Sci.* 317, 1095–1148. doi:10.2475/10.2017.02

Watson, E. B., and Harrison, T. M. (2005). Zircon thermometer reveals minimum melting conditions on earliest earth. *Science* 308, 841–844. doi:10.1126/science.1110873

Wu, F.-Y., Lin, J.-Q., Wilde, S. A., Zhang, X. O., and Yang, J.-H. (2005). Nature and significance of the Early Cretaceous giant igneous event in eastern China. *Earth Planet. Sci. Lett.* 233, 103–119. doi:10.1016/j.epsl.2005.02.019

Wu, F., Yang, J., Xu, Y., Wilde, S. A., and Walker, R. J. (2019). Destruction of the North China craton in the mesozoic. *Annu. Rev. Earth Planet. Sci.* 47, 173–195. doi:10.1146/annurev-earth-053018-060342

Liu, X., Jin, W., Li, S., and Xu, X. (1993). Two types of Precambrian high-grade metamorphism, Inner Mongolia, China. *J. Metamorph. Geol.* 11, 499–510. doi:10.1111/j.1525-1314.1993.tb00167.x

Xu, Y. G. (2001). Thermo-tectonic destruction of the archaean lithospheric keel beneath the sino-Korean craton in China: Evidence, timing and mechanism. *Phys. Chem. Earth, Part A Solid Earth Geodesy* 26, 747–757. doi:10.1016/s1464-1895(01)00124-7

Xu, Y., Li, H., Pang, C., and He, B. (2009). On the timing and duration of the destruction of the North China Craton. *Chin. Sci. Bull.* 54, 3379–3396. doi:10.1007/s11434-009-0346-5

Xue, F., Santosh, M., Kim, S. W., Tsunogae, T., and Yang, F. (2021). Thermo-mechanical destruction of archean cratonic roots: Insights from the mesozoic laiyuan granitoid complex, North China craton. *Lithos* 400-401, 106394. doi:10.1016/j.lithos.2021.106394

Xue, F., Santosh, M., Tsunogae, T., and Yang, F. (2019). Geochemical and isotopic imprints of early cretaceous mafic and felsic dyke suites track lithosphere-asthenosphere interaction and craton destruction in the North China Craton. *Lithos* 326-327, 174–199. doi:10.1016/j.lithos.2018.12.013

Yang, F., Santosh, M., and Kim, S. W. (2018a). Mesozoic magmatism in the eastern North China Craton: Insights on tectonic cycles associated with progressive craton destruction. *Gondwana Res.* 60, 153–178. doi:10.1016/j.gr.2018.04.003

Yang, F., Santosh, M., and Tang, L. (2018b). Extensive crustal melting during craton destruction: Evidence from the Mesozoic magmatic suite of Junan, eastern North China Craton. *J. Asian Earth Sci.* 157, 119–140. doi:10.1016/j.jseaes.2017.07.010

Yang, J.-H., Zhang, M., and Wu, F.-Y. (2018c). Mesozoic decratonization of the North China Craton by lithospheric delamination: Evidence from Sr-Nd-Hf-Os isotopes of mantle xenoliths of Cenozoic alkaline basalts in Yangyuan, Hebei Province, China. *J. Asian Earth Sci.* 160, 396–407. doi:10.1016/j.jseaes.2017.09.002

Yang, J., Sun, J., Zhang, J., and Wilde, S. A. (2012a). Petrogenesis of Late Triassic intrusive rocks in the northern Liaodong Peninsula related to decratonization of the

North China Craton: Zircon U–Pb age and Hf–O isotope evidence. *Lithos* 153, 108–128. doi:10.1016/j.lithos.2012.06.023

Yang, K. F., Fan, H. R., Santosh, M., Hu, F. F., Wilde, S. A., Lan, T. G., et al. (2012b). Reactivation of the Archean lower crust: Implications for zircon geochronology, elemental and Sr–Nd–Hf isotopic geochemistry of late Mesozoic granitoids from northwestern Jiaodong Terrane, the North China Craton. *Lithos s.* 146–147, 112–127. doi:10.1016/j.lithos.2012.04.035

Yu, P.-P., Weinberg, R. F., Zheng, Y., and Finch, M. A. (2022). Multiple crustal melting pulses and Hf systematics in zircons. *Lithos* 410-411, 106583. doi:10.1016/j.lithos.2021.106583

Yu, P., Zhang, Y., Zhou, Y., Weinberg, R. F., Zheng, Y., and Yang, W. (2019). Melt evolution of crustal anatexis recorded by the Early Paleozoic Baiyunshan migmatite-granite suite in South China. *Lithos* 332-333, 83–98. doi:10.1016/j.lithos.2019.02.020

Zhang, Q., Wang, Y., Jin, W., and Li, C. (2008). Eastern China plateau during the late mesozoic: Evidence, problems and implication. *Geol. Bull. China* 27, 1404–1430.

Zhang, Z., Teng, J., Romanelli, F., Braitenberg, C., Ding, Z., Zhang, X., et al. (2014). Geophysical constraints on the link between cratonization and orogeny: Evidence from the Tibetan plateau and the North China craton. *Earth-Science Rev.* 130, 1–48. doi:10.1016/j.earscirev.2013.12.005

Zhao, G., Sun, M., Wilde, S. A., and Li, S. (2005). Late archean to paleoproterozoic evolution of the North China craton: Key issues revisited. *Precambrian Res.* 136, 177–202. doi:10.1016/j.precamres.2004.10.002

Zhao, G., Wilde, S. A., Sun, M., Guo, J., Kröner, A., Li, S., et al. (2008). SHRIMP U–Pb zircon geochronology of the huai'an complex: Constraints on late archean to paleoproterozoic magmatic and metamorphic events in the Trans-North China orogen. *Am. J. Sci.* 308, 270–303. doi:10.2475/03.2008.04

Zheng, J., Xia, B., Dai, H., and Ma, Q. (2021). Lithospheric structure and evolution of the North China Craton: An integrated study of geophysical and xenolith data. *Sci. China Earth Sci.* 64, 205–219. doi:10.1007/s11430-020-9682-5

Zhu, G., Liu, G. S., Niu, M. L., Xie, C. L., Wang, Y. S., and Xiang, B. (2009). Syn-collisional transform faulting of the Tan-Lu fault zone, East China. *Int. J. Earth Sci.* 98, 135–155. doi:10.1007/s00531-007-0225-8

Zhu, R., Zhang, H., Zhu, G., Meng, Q., Fan, H., Yang, J., et al. (2017). Craton destruction and related resources. *Int. J. Earth Sci.* 106, 2233–2257. doi:10.1007/s00531-016-1441-x

Zou, X., Qin, K., Han, X., Li, G., Evans, N. J., Li, Z., et al. (2019). Insight into zircon REE oxy-barometers: A lattice strain model perspective. *Earth Planet. Sci. Lett.* 506, 87–96. doi:10.1016/j.epsl.2018.10.031